Core effect on the diamagnetic spectrum of barium Rydberg states

H. F. Yang,[1,2] W. Gao,[1,2] W. Quan,[1] X. J. Liu,[1] and H. P. Liu[1,*]

[1]*State Key Laboratory of Magnetic Resonance and Atomic and Molecular Physics, Wuhan Institute of Physics and Mathematics, Chinese Academy of Sciences, Wuhan 430071, People's Republic of China*

[2]*Graduate School of the Chinese Academy of Sciences, Beijing 100049, People's Republic of China*

(Received 18 January 2012; published 6 March 2012)

We study the core effect of nonhydrogenic alkaline-earth-metal barium in its diamagnetic spectrum by one photon transition from the ground state $6s^2\,{}^1S_0$ experimentally and theoretically. The non-Coulombic potential of the ion core introduces an extra energy shift compared with hydrogen and a level anticrossing between different n manifolds, characterized by the quantum defect of the concerned angular momentum states. With a complex rotation coordinate technique and a B-spline expansion method, we develop a matrix-form Hamiltonian based on an effective potential incorporating the angular-dependent quantum defect into the angular rotation term. The nonhydrogen core effects are investigated by sweeping the quantum defects of different channels in the calculation. Results show that quantum defects of p and f states have a undeniable effect on the intensities and positions of the spectral lines, although barium is closely hydrogenlike in the energy range examined. The anticrossing spectral lines are also identified with the aid of theoretical calculations. The calculations are in good agreement with the experimental observations.

DOI: 10.1103/PhysRevA.85.032508 PACS number(s): 32.30.Jc, 32.60.+i, 32.80.Ee, 31.15.−p

I. INTRODUCTION

The Rydberg atom in a magnetic field, one of the simplest realizations of a classically chaotic system, has been studied for many years. In a pure magnetic field, the system has a rotational symmetry about the direction of the magnetic field. We can separate this orbital angular motion perpendicular to the magnetic field easily and reduce the problem to a two-dimensional one. For a low-lying atom in a weak magnetic field, the quadratic Zeeman term (usually called the diamagnetic term) is negligible. With the increase of magnetic intensity, however, the diamagnetic potential will compare with or dominate the Coulomb potential and the system will gradually change from order to chaos [1].

Early in the 1930s, the experiment on atomic diamagnetism by Jenkins and Segrè was among the first in which the Rydberg atoms in magnetic field were exploited [2]. In an accompanying paper, Schiff and Snyder attempted to obtain a theoretical understanding of the data [3]. Thirty years later, Garton and Tomkins revisited the topic in 1969 and observed the unexpected quasi-Landau resonances [4]. After that, experimental investigations of the quadratic Zeeman effect [5–10] concentrating on hydrogen and hydrogenlike atoms have been done in an attempt to uncover the dynamics underlying the simplest possible magnetic field spectrum, and the relevant theoretical efforts [11–13] in that direction have produced good agreement with the experiments.

Specifically, the alkaline earth atoms such as barium and strontium played an important role in the understanding of the behavior of atoms in high magnetic fields for their complexity far beyond hydrogen and hydrogenlike atoms. In the alkaline-earth metals, the doubly excited states appear as prominent perturbation of the principal series in magnetic field [4,14–16], or even in the absence of external fields [17,18], resulting in the quantum defect being energy dependent [19,20]. Therefore, there is a new possibility of competition between the electronic correlations and the external field which renders these spectra very interesting [21]. Typically, Fonck *et al.* [14] observed the diamagnetic effect in $6s6p\,{}^1P_1-6sns\,{}^1S_0$ Rydberg series of barium in magnetic fields of 2–4 T and found that the perturbation of this series by the $5d7d\,{}^1S_0$ level reduces the shift below the hydrogenic value. Lu *et al.* [15] presented a densitometer mapping of diamagnetic effects on barium and strontium and discussed the effects of perturbation states ($4d5p\,{}^1P_1$ for strontium and $5d8p\,{}^1P_1$ for barium) on the intensity and spacing of principle series spectra. The group of Connerade in Imperial College contributed much to the investigations of the diamagnetic effect of alkaline earths [21–25], giving a lot of inspiration to our work on the core scattering of the quadratic Zeeman spectrum of barium [26].

The more interesting factor is the level of anticrossings of Rydberg atoms in the external field introduced by the nonhydrogenic Coulomb potential. Hydrogen atoms have a higher dynamics symmetry SO(4), and the states within the same n manifold are degenerate. If an external electric field is applied, the energy levels from different n manifolds will meet and cross but they do not interact, and the spectral lines go in their own ways with the field applied. For hydrogen atoms in a magnetic field, the inseparability of the system due to the diamagnetic term will result in anticrossings for levels, but it is negligible for high Rydberg states [27]. In the case of the nonhydrogenic atoms, however, the ion core cannot be treated as a geometric point and the core potential deviates from Coulombic form. Its charge distribution in finite geometric space, although the size is small, will break the dynamics symmetry and make the system inseparable. In this case, the levels with the same parity from different n manifolds will suffer from anticrossings rather than a direct crossing without interaction, even in an electric field. The nonhydrogen core is related to the phase shift of the hydrogen wave function for the specified angular momentum state, a partial wave phase shift which is characterized by the terminology

*liuhongping@wipm.ac.cn

"quantum defect." The anticrossings play a significant role for the atomic spectrum in an external field [28–30]. The theoretical calculation of anticrossings can reveal important dynamics information such as inelastic core scattering between different quantum channels. However, the positions and widths of anticrossing have a sensitive dependence on the wave functions chosen [28], and the theoretical calculation for such systems serves as a stringent approach to test the accuracy of approximate wave functions and the validity of the method used [29]. A high precision and reliability is also in demand for the related experiments.

In this paper we investigate the nonhydrogenic core effect of barium by directly recording the diamagnetic spectrum and comparing it with the quantum-mechanical calculation considering the quantum defects from different orbital angular momentum under an "l-truncation" approximation [31]. In the quantum-mechanical calculations, we can switch the specified channel(s) on or off, enabling us to see the direct contribution(s) for the spectrum. At the same time, careful attention is paid to the energy dependence of the quantum defects. It can extract more information than previous theoretical calculations [19,20,32]. In our case, barium is irradiated to $6snp$ Rydberg states directly from the ground state by single-photon excitation. The core effect is incarnated on the transitions from the ground state to the p component of the mixing excited states under external magnetic field. The one-photon transition selection confines the channels $p, f, \ldots$ to participate in the interaction, but only the former two states have observable effects for their considerable nonzero quantum defects.

II. EXPERIMENTAL

The experimental apparatus is described in our previous work [26], and some improvements have been made in the present measurement. An atom beam produced from an atom oven travels to the interacting point, intersecting with the laser beam at a small angle of 15° in the center of the superconductor magnet (Oxford Instruments). The oven is a stainless chamber heated to about 700 °C by a multicycle solenoid resistance at current of 2 A, instead of the previous nickel-chrome alloy tube heated directly by its resistance under large current of about 130 A. The present atom beam is much more stable than before. Two pinholes are inserted between the atomic oven and the interacting point to collimate the atomic beam. The interacting point is situated between a pair of electric Stark plates parallel to the magnetic field, where an additional electric field can be applied. Rather than taking the superconductor cavity as our atomic chamber, we improve it to a much smaller one for efficient pumping. One photon corresponding to 238 nm is used to excite the barium atom from the ground state to a high Rydberg state $6snp$ and a pair of electric grids is used to ionize the excited Rydberg atom. The ionized residual is detected by a pair of microchannel plates mounted at the end of the chamber. The signal is recorded by an oscilloscope (Tektronix TDS1012), and the digital data stream is transferred to a personal computer for real-time signal processing.

The laser beam is produced by a dye laser system (Lambda Physik, Scanmate 2E) pumped by a Nd:YAG laser (Spectra Physics) where an etalon is inserted in the oscillator cavity to narrow the linewidth down to 0.9 GHz. The laser beam from the dye laser is frequency-doubled by a system-controlled beta barium borate crystal and the dichromatic beams are separated by two pairs of prisms. A Soleil-Babinet compensator is used to rotate the laser from horizontal polarization to vertical or circular polarization. The wavelength is monitored by a Burleigh wavemeter and its scanning is controlled by the same personal computer. The superconducting solenoid we used can produce a magnetic field up to 5 T and sweep with stability of better than one in ten thousand.

III. THEORETICAL CALCULATION

In the presence of a pure magnetic field, the Hamiltonian H for Rydberg barium atom, in atomic units, can be written as follows:

$$H = \frac{p^2}{2} + V_r + \frac{B}{2}L_z + \frac{B^2}{8}r^2\sin^2\theta, \tag{1}$$

where B is the magnetic field strength in atomic units and θ the angle coordinate of a Rydberg electron in spherical coordinates, the terms $\frac{B}{2}L_z$ and $\frac{B^2}{8}r^2\sin^2\theta$ are the paramagnetic term and diamagnetic term, respectively, and V_r is the Coulomb potential considering the effects of valence electron polarization of the core system. The term V_r deviates from the form of $-\frac{1}{r}$ at small values of r. The complexity of the core-induced electron screening makes the Schrödinger equation for the nonhydrogen centrifugal problem lose analyticity. In this case, the term V_r is usually expressed by model potential, parameterized by some angular momentum-dependent variables which are closely correlated with quantum defects. Rather than using the model potential V_r [33] or the R-matrix method including the quantum defects implicitly [34], we employ an equivalent form for the central field potential:

$$V_r = \frac{\lambda(\lambda+1) - l(l+1)}{2r^2} - \frac{1}{r}, \tag{2}$$

where $\lambda = l - \delta + \mathrm{int}(\delta)$ and the quantum defects are explicitly enclosed. Here $\mathrm{int}(\delta)$ is the rounded nearest-integer value of the quantum defect. Another benefit for this formula in Eq. (2) for the potential is that the Schrödinger equation has an analytic solution for its eigenfunctions [35]. We employ a reduced quantum defect

$$\delta' = \delta - \mathrm{int}(\delta) \tag{3}$$

to quantificationally describe the real contribution of the quantum defect for a given angular momentum channel. In the following text, we will use δ' rather than δ and ignore the prime.

In this way, the Hamiltonian of atom in external magnetic field can be expressed by a full matrix on the basis of the second Whittaker functions [35], which are called quantum defect orbitals, making it possible to perform a multichannel quantum defect theory (MQDT) based calculation. In the present work, we will take the B-spline function as the basis instead of the quantum defect orbitals. The main excuse is that the Hamiltonian in B-spline basis has a symmetric banded matrix form. This special matrix structure will save much time in numerical diagonalization to obtain the final eigenvalues and eigenfunctions. In addition, the complex coordinate is

employed in our calculation. This method will supply complex eigenvalues with their imaginary parts corresponding to the natural linewidths of the absorption. In the case of pure magnetic fields, the radial wave function of the system can be expanded in terms of a B-spline basis as

$$R_n(r) = \sum_i C_i^n B_i^k(r), \tag{4}$$

where $B_i^k(r)$ is the ith B spline of order k defined in Refs. [36–38], while the angular wave function is expanded in spherical harmonic functions. It should be noted that the parity symmetry π_z is not considered in our calculation. This indifferent processing enables us to incorporate the Stark term in the electric field into the same program code.

Since the σ^+ and σ^- polarized diamagnetic spectrums are completely identical after a proper shift [23], only the σ^+ spectrum is presented in this paper. Quantum defects of $\delta_s = 0.2572$, $\delta_d = -0.25$, and $\delta_f = 0.04$ are used during the calculation if not specified, while δ_p is varied in a small range.

IV. RESULTS AND DISCUSSION

The σ^+-polarized diamagnetic spectrum of barium in various magnetic fields $B = 1$, 1.7, 3, and 4 T are shown in Figs. 1(a)–1(e). The upper and lower panels show the calculated spectrum and the experimental observation, respectively. Spectra in Figs. 1(a)–1(c) are shown in the same energy scale, $-100 \sim -70$ cm^{-1}, ranging from l mixing ($B = 1$ T) to n mixing ($B = 3$ T). The spectra at higher magnetic field $B =$ 4 T within an extended energy range in Figs. 1(d)–1(e) show the n mixing of the diamagnetic structure as well as the quantum defect dependence roundly.

The spectral lines in the same n manifold shift to higher energy when the magnetic field gets stronger and stronger, due to the diamagnetic interaction. According to the Pauli quantization scheme [25], the energy shift of p states can be estimated by

$$\delta E \sim \left(\frac{1}{2} + \frac{3n^4 B}{8}\right)\delta_B, \tag{5}$$

where we can see that the energy shift is proportional to the magnetic field strength. For $n = 38$, as indicated in the spectrum, the energy shift from $B = 1$–1.7 T is estimated to be around 3 cm^{-1} and that for $B = 1.7$–3 T is around 9 cm^{-1}, approaching the experimental observations.

Another interesting point is the spectral line splittings within the same n manifold, which are degenerate at zero field. These splittings are due to the l mixing between different angular momentum states of the same parity induced by the diamagnetic term. For the spectrum at a specified magnetic field, the splitting gets larger at higher energies. At relatively low field ($B = 1$ T), for example, the spectral lines at small principal quantum number $n = 38$ gather closely but they begin to be distinguishable at higher energies. The dependence of line splitting on the magnetic fields can be clarified by comparing the spectrum at different magnetic fields, as shown in Figs. 1(a)–1(c). When the magnetic field increases to 1.7 T, different l states with the same parity interact more seriously due to the contribution of the magnetic field, and the line splitting gets so large that the satellites can be distinguished

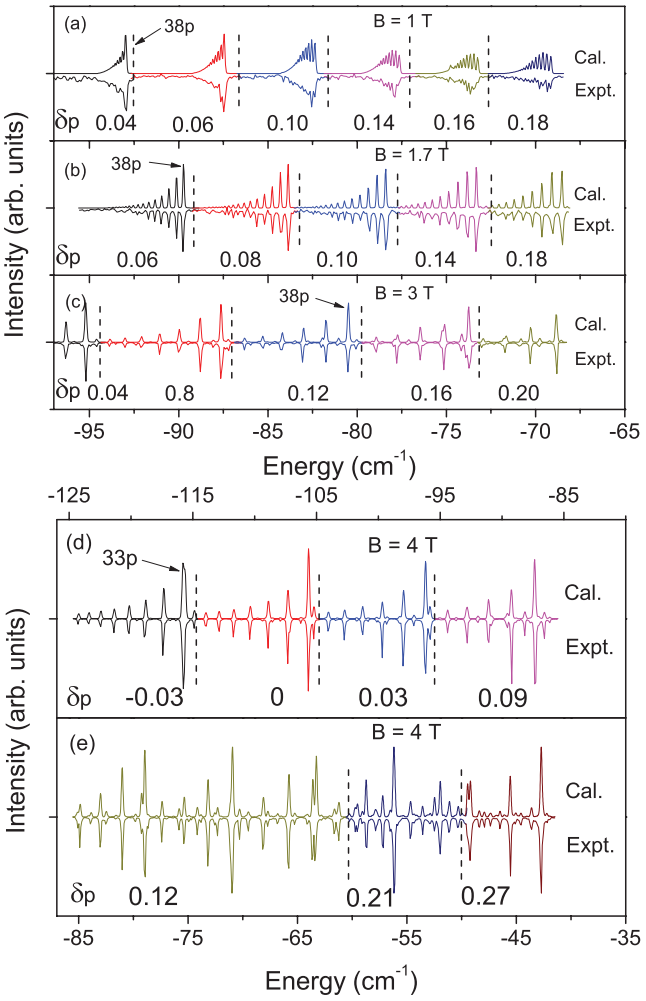

FIG. 1. (Color online) The calculated (upper panel) and experimental (lower panel) σ^+-polarized diamagnetic spectra of barium at various magnetic field strengths: $B = 1$, 1.7, 3, and 4 T. The calculation has considered the quantum defects of channels $6snp$, $6snd$, and $6snf$ with fixed reduced quantum defects $\delta_s = 0.2572$, $\delta_d = -0.25$, and $\delta_f = 0.04$. The reduced quantum defect δ_p of channel $6snp$ is energy dependent and takes different values for different energy ranges.

clearly, even at lower energies. When it comes to 3 T, the manifolds of adjacent n overlap with each other, indicating the spectrum goes into the n-mixing region. There is no analytical expression to calculate the level separation within one manifold at a certain magnetic field, but we can see that the separation is approximately equal and gets slightly smaller at lower energy in the same manifold, which coincides with the conclusion of van der Veldt *et al.* [39].

The effect of quantum defects on the spectra of barium is also worth our attention. Since the value of the reduced quantum defect for p states is almost zero in the examined energy range, the zero-field states with odd parity are nearly degenerate, resulting the line positions and intensities of the mixed states having a nearly regular structure. It is similar to the case of hydrogen [40], but different from the case of strontium in a magnetic field of 2.465 T, where the quantum defect of the p channel is large enough to separate the

p component from the satellites of higher l partial waves ($l \geqslant 3$) in the same manifold [24]. We will return to the discussion about the effect of the quantum defect δ_p on the diamagnetic spectrum later.

A quantum calculation for barium in the magnetic field corresponding to the observations is also presented in Fig. 1. The quantum defects of channels $6sns$, $6snd$, and $6snf$ are fixed at values $\delta_s = 0.2572$, $\delta_d = -0.25$, and $\delta_f = 0.04$, which are obtained by fitting the experimental observations in Ref. [41]. They are nearly independent of the principal quantum number n and are kept constant in the energy range of interest. On the contrary, the quantum defect for channel $6snp$ varies along with energy or n, making it difficult to treat in the calculation.

As the spectrum in external fields is very sensitive to the quantum defect, we perform MQDT calculations at sweeping δ_p with an appropriate step. For example, Fig. 2(a) displays how we obtain the calculated spectrum shown in Figs. 1(d)–1(e) at magnetic field of 4 T. The upper panels in each row in Fig. 2(a) are the spectra calculated at a series of quantum defect values δ_p. We can find that in a certain energy range (separated by dash lines) with a certain quantum defect, the calculated positions of the lines, especially for the dominant peaks, match the experimental ones. The best agreements for the dominant peaks are circled in Fig. 2. At $B = 4$ T, for example, for the $n = 35$ dominant line, at the quantum defect $\delta_p = 0.03$ only, can we reach the best agreement with each other.

In order to study how δ_p takes effect in the diamagnetic spectrum, a part of Fig. 2(a) is magnified into Fig. 2(b). For the case of barium, although its quantum defect of the p state is nearly an integer for the energy region involved here, it has a undeniable influence upon the position and intensity of the spectrum. The peaks are labeled k, which is used by Gay and Delande to distinguish the diamagnetic states [42]. The expression $k = 0$ indicates the predominant peak corresponding to the $33p$ state, and $k = 2,4,6,\ldots$ for the satellites. The calculated peaks with the same k labels at various values of δ_p are linked by dashed lines to guide the eye. As the δ_p increases from -0.03 to 0.09, the peaks predominated by p move toward lower energy much faster than the satellites with higher k. This indicates that the quantum defect of p states has a predominant effect on peak $k = 0$ and makes little contribution to the peaks with higher k values. In contrast, it can also help us to determine the best quantum defect value of p states at a specified energy range.

With the method presented in Fig. 2, the calculations for the diamagnetic spectra at various magnetic fields can be performed as shown in Fig. 1. In the calculation, the quantum defect of channel $6snp$ varies from $\delta_p = -0.03$ at $E = -125$ cm^{-1} to $\delta_p = 0.27$ at $E = -45$ cm^{-1}. It can be seen that the calculated spectra in the upper panels are in excellent agreement with the experimental observation in the lower panel.

In order to investigate the effect of the f-state quantum defect on the spectrum, the calculations at sweeping δ_f are also performed, which are shown in Fig. 3. We can see from Fig. 3(a) that with increasing δ_f, the peak with $(n,k) = (35,10)$ shifts to lower energy. The (35,12) peak should have the same shifting magnitude as (35,10). However, as shown in Fig. 3(a), the shifting of peak (35,12) is seriously depressed

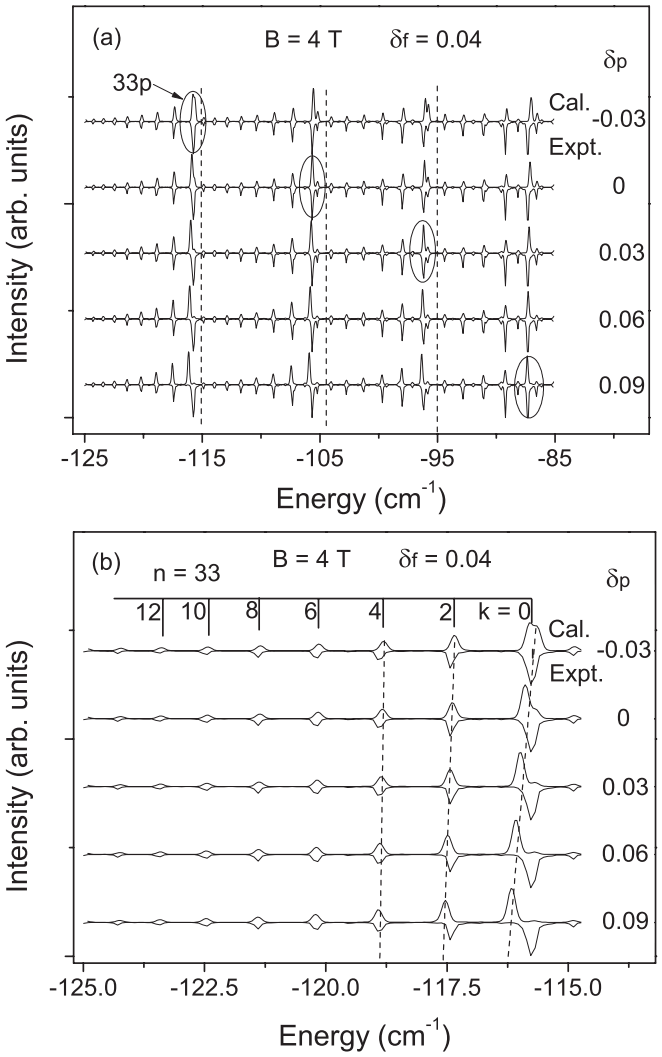

FIG. 2. The effect of quantum defect δ_p on the diamagnetic spectrum. (a) The spectra calculated at quantum defects varying from $\delta_p = -0.03$ to $\delta_p = 0.09$ while other quantum defects are kept as the "standard" values used in Fig. 1. The comparison is made taking the experimental observation as reference. The coincidence between theory and experiment "requires" the quantum defect of $6snp$ to vary with the energy as indicated by the circled lines. (b) The magnification in a narrow energy range of (a). The peaks in the same n manifold are labeled by k. See text for the detail.

by the intruding repelling interaction from p state (34,0). On the contrary, the p state is recoiled to lower energy with acceleration. Generally speaking, the quantum defect of f states has a much stronger effect on the high-k states than the p-predominant ones [24]. In our case, the diamagnetic effect makes some higher-k states of higher n manifold intrude toward lower energy and "collide" with the p-predominant peak ($k = 0$) in the neighborhood of a lower principal quantum state $n - 1$. If there are nonzero reduced quantum defects for these two angular momentum states, the two colliding states will suffer an anticrossing. The core-induced interaction will repel the concerned spectral lines, for example, here the peaks (34,0) and (35,12).

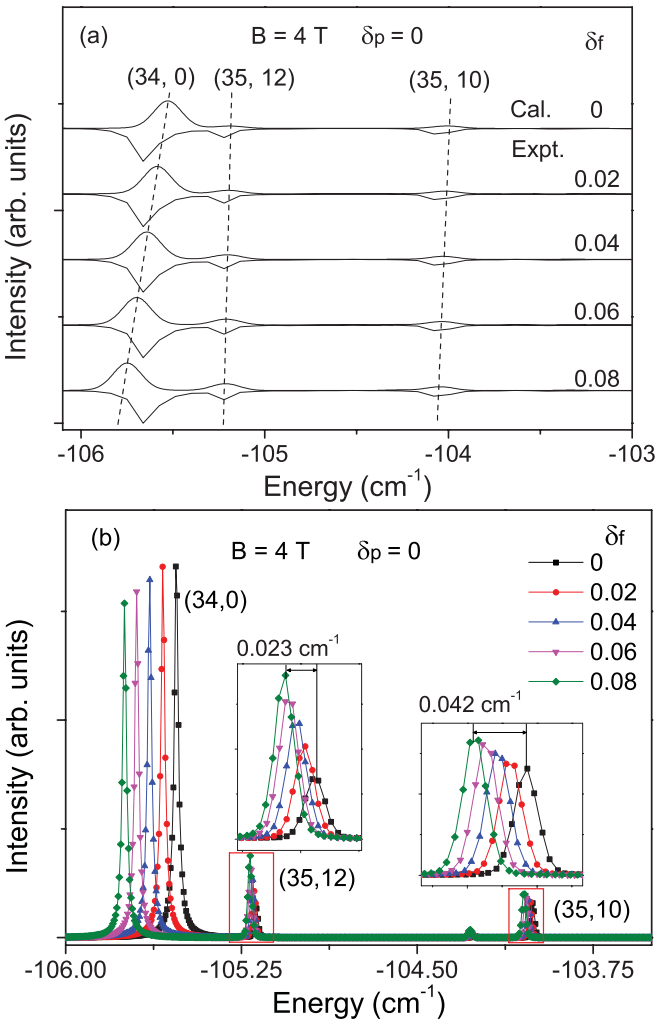

FIG. 3. (Color online) The effect of quantum defect δ_f on the diamagnetic spectrum. (a) The calculated (upper panel) and experimental spectrum (lower panel) at a sweeping quantum defect of f state. An interaction between a pair of closely neighboring spectral lines can be confirmed by line position shifts as δ_f. The interaction states are the p-predominant $k = 0$ state and the intruding higher-k state from the higher neighboring n manifold. One can also reach this conclusion by tracing the spectral line intensities with the higher-resolution spectrum by giving up the experimental Gauss broadening as shown in (b). The spectral lines are labeled by (n,k).

This quantum-defect-induced interaction can also be revealed by analyzing the spectral line intensities at different quantum defect values of δ_f as shown in Fig. 3(b). In Fig. 3(a), an appropriate Gauss broadening ($\Delta\upsilon = 0.03\ \mathrm{cm}^{-1}$) is adopted to convolute with the calculated spectrum due to the laser linewidth and Doppler broadening, which conceal the fine variation in the spectral line intensity and position. The calculation for Fig. 3(b) is the same as that in Fig. 3(a), but a narrow broadening is considered to recover the interaction details. It can be seen that the (35,10) peak shifts to lower energy at about $0.042\ \mathrm{cm}^{-1}$ while the shifting of the peak (35,12) is depressed, only about $0.023\ \mathrm{cm}^{-1}$. The p-predominant peak (34,0) is obviously repealed by its neighbor colliding partner. The interaction information can also be deduced from the intensity variation of the calculated spectral lines. For the peak (35,10), the intensity variation is very small, indicating a weak interaction from other states, while for the peak (35,12), the intensity variation is much more acute. This can be well understood by its strong interaction with the closest neighbor state (34,0). We label the wave functions of states (35,10), (35,12), and (34,0) as $\varphi_i (i = 0,1,2)$ ($\sum_i |\varphi_i|^2 = 1$), which constitutes a small interaction space. With the increase of the quantum defect of δ_f, the intensity enhancement of spectral line (35,12) and the intensity lessening for (34,0) shows that states φ_2 and φ_3 mix violently with each other, resulting in the final state containing more components of state φ_2.

In our calculation, the choice of quantum defect values of s and d channels does not affect the diamagnetic spectrum at all. This is well understood by the matrix element of the Hamiltonian. The diamagnetic term couples the states with $\Delta L = \pm 2$ only. For our excitation scheme of one-photon irradiation from the ground state $6s^2\ ^1S_0$, the circularly polarized laser permits the transition to $6snp$, keeping the contribution of quantum defects of s and d states in vain. These transition selection tricks enable us to pick up or prohibit the participation of concerned states.

V. CONCLUSION

In this paper, the σ^+-polarized diamagnetic spectrum is studied in l-mixing and n-mixing regions experimentally and theoretically. The odd-parity Rydberg states are populated by one-photon transition from the ground state $6s^2\ ^1S_0$. General properties of the diamagnetic spectrum have been reinvestigated. In addition, based on the complex rotation coordinate technique and B-spline expansion method, we performed quantum mechanical calculations for the diamagnetic spectrum with the quantum defects of multichannels considered. By sweeping the quantum defect of the specified channel in the calculation, we find that the quantum defects of p and f states have a undeniable effect on the intensities and positions of the diamagnetic spectral lines, although barium is closely hydrogenlike. The slightly increasing quantum defects of the p channel from -0.03 to 0.09 result in a significant shift of the predominant peak ($k = 0$) in one n manifold. When scanning the quantum defect of channel f from 0 to 0.08 in the calculation, we find a pair of spectral lines closely interrelated. By investigating the spectral line positions and intensities with the quantum defect of channel f, the pair of lines is identified to originate from two interacting states with their energy levels anticrossing. The spectral line position is very sensitive to the quantum defect of channel f. In contrast, we can also use the sweeping method to accurately determine the quantum defect values in the specified energy range.

ACKNOWLEDGMENTS

One of the authors, H.P.L., thanks Prof. Connerade at Imperial College for his encouragement. This work is supported by the National Natural Science Foundation of China (NSFC) under Grants No. 11174329 and No. 91121005.

[1] K. Ganesan and R. Gębarowski, Pramana-J Phys. **48**, 379 (1997).
[2] F. A. Jenkins and E. Segrè, Phys. Rev. **55**, 52 (1939).
[3] L. I. Schiff and H. Snyder, Phys. Rev. **55**, 59 (1939).
[4] W. R. S. Garton and F. S. Tomkins, Astrophys. J. **158**, 839 (1969).
[5] K. T. Lu, F. S. Tomkins, H. M. Crosswhite, and H. Crosswhite, Phys. Rev. Lett. **41**, 1034 (1978).
[6] P. F. O′Mahony and K. T. Taylor, J. Phys. B **19**, L65 (1986).
[7] A. Holle, G. Wiebusch, J. Main, K. H. Welge, G. Zeller, G. Wunner, T. Ertl, and H. Ruder, Z. Phys. D **5**, 279 (1987).
[8] P. Cacciani, S. Liberman, E. Luc-Koenig, J. Pinard, and C. Thomas, J. Phys. B **21**, 3473 (1988).
[9] C. H. Iu, G. R. Welch, M. M. Kash, L. Hsu, and D. Kleppner, Phys. Rev. Lett. **63**, 1133 (1989).
[10] P. F. O′Mahony, Phys. Rev. Lett. **63**, 2653 (1989).
[11] C. H. Iu, G. R. Welch, M. M. Kash, D. Kleppner, D. Delande, and J. C. Gay, Phys. Rev. Lett. **66**, 145 (1991).
[12] P. F. O′Mahony and F. Mota-Furtado, Phys. Rev. Lett. **67**, 2283 (1991).
[13] S. Watanabe and H. A. Komine, Phys. Rev. Lett. **67**, 3227 (1991).
[14] R. J. Fonck, F. L. Roesler, D. H. Tracy, K. T. Lu, F. S. Tomkins, and W. R. S. Garton, Phys. Rev. Lett. **39**, 1513 (1977).
[15] K. T. Lu, F. S. Tomkins, and W. R. S. Garton, Proc. R. Soc. London A **362**, 421 (1978).
[16] W. R. S. Garton, F. S. Tomkins, and H. M. Crosswhite, Proc. R. Soc. London A **373**, 189 (1980).
[17] W. R. S. Garton and K. Codling, Proc. Phys. Soc. London **75**, 87 (1960).
[18] J. P. Connerade and A. M. Lane, Rep. Prog. Phys. **51**, 1439 (1988).
[19] M. H. Halley, D. Delande, and K. T. Taylor, J. Phys. B **26**, 1775 (1993).
[20] H. Y. Meng, J. At. Molec. Sci. **2**, 58 (2011).
[21] G. Droungas, N. E. Karapanagioti, and J. P. Connerade, Phys. Rev. A **51**, 191 (1995).
[22] J. P. Connerade, G. Droungas, R. Elliott, X. He, N. Karapanagioti, M. A. Farooq, H. Ma, J. P. Marangos, and M. Nawaz, J. Phys. B **27**, 2753 (1994).
[23] R. J. Elliott, G. Droungas, and J. P. Connerade, J. Phys. B **28**, L537 (1995).
[24] R. J. Elliott, G. Droungas, J. P. Connerade, X. H. He, and K. T. Taylor, J. Phys. B **29**, 3341 (1996).
[25] J. P. Connerade, G. Droungas, N. E. Karapanagioti, and M. S. Zhan, J. Phys. B **30**, 2047 (1997).
[26] H. P. Liu, W. Quan, L. Shen, J. P. Connerade, and M. S. Zhan, Phys. Rev. A **76**, 013412 (2007).
[27] M. L. Zimmerman, M. M. Kash, and D. Kleppner, Phys. Rev. Lett. **45**, 1092 (1980).
[28] P. Cacciani, S. Liberman, E. Luc-Koenig, J. Pinard, and C. Thomas, Phys. Rev. A **40**, 3026 (1989).
[29] Y. Li, Theor. Chem. Acc. **117**, 163 (2007).
[30] R. C. Stoneman, G. Janik, and T. F. Gallagher, Phys. Rev. A **34**, 2952 (1986).
[31] P. A. Braun, J. Phys. B **18**, 4187 (1985).
[32] P. F. O′Mahony and K. T. Taylor, Phys. Rev. Lett. **57**, 2931 (1986).
[33] H. Y. Meng and T. Y. Shi, Commun. Theor. Phys. **52**, 333 (2009).
[34] J. G. Rao and K. T. Taylor, J. Phys. B **30**, 3627 (1997).
[35] G. Simons, J. Chem. Phys. **60**, 645 (1974).
[36] I. J. Schoenberg, Q. Appl. Math. **4**, 45 (1946).
[37] C. De Boor, J. Approx. Theory **6**, 50 (1972).
[38] H. Bachau, E. Cormier, P. Decleva, J. E. Hansen, and F. Martn, Rep. Prog. Phys. **64**, 1815 (2001).
[39] T. van der Veldt, W. Vassen, and W. Hogervorst, J. Phys. B **25**, 3295 (1992).
[40] C. W. Clark and K. T. Taylor, Nature (London) **292**, 437 (1981).
[41] M. Aymar, P. Camus, M. Dieulin, and C. Morillon, Phys. Rev. A **18**, 2173 (1978).
[42] J. C. Gay and D. Delande, Comments At. Mol. Phys. **13**, 275 (1983).